

Spin excitations arising from anisotropic Dirac spinons in $\text{YCu}_3(\text{OD})_6\text{Br}_2[\text{Br}_{0.33}(\text{OD})_{0.67}]$

Lankun Han,^{1,2} Zhenyuan Zeng,^{1,2} Chengkang Zhou,³ Bo Liu,¹ Maiko Kofu,⁴ Kenji Nakajima,^{4,*} Paul Steffens,⁵ Arno Hiess,⁵ Zi Yang Meng,³ Yixi Su,^{6,†} and Shiliang Li^{1,2,‡}

¹*Beijing National Laboratory for Condensed Matter Physics,*

Institute of Physics, Chinese Academy of Sciences, Beijing 100190, China

²*School of Physical Sciences, University of Chinese Academy of Sciences, Beijing 100190, China*

³*Department of Physics and HK Institute of Quantum Science & Technology,*

The University of Hong Kong, Pokfulam Road, Hong Kong

⁴*J-PARC Center, Japan Atomic Energy Agency, Tokai, Japan*

⁵*Institut Laue-Langevin, 71 Avenue des Martyrs, 38000 Grenoble, France*

⁶*Jülich Centre for Neutron Science (JCNS) at Heinz Maier-Leibnitz Zentrum (MLZ),
Forschungszentrum Jülich, Lichtenbergstrasse 1, 85747 Garching, Germany*

A Dirac quantum spin liquid hosts Dirac spinons, which are low-energy fractionalized neutral quasiparticles with spin 1/2 that obey the Dirac equation. Recent inelastic neutron scattering studies have revealed cone spin continuum in $\text{YCu}_3(\text{OD})_6\text{Br}_2[\text{Br}_x(\text{OD})_{1-x}]$, consistent with the convolution of two Dirac spinons. In this work, we further studied spin excitations using the inelastic neutron scattering technique. The width of low-energy spin excitations shows a linear temperature dependence, which can be explained by spinon-spinon interactions with a Dirac dispersion. Polarized neutron scattering measurements reveal that in-plane magnetic fluctuations are about 1.5 times stronger than the out-of-plane ones, suggesting the presence of Dzyaloshinskii-Moriya interaction and consistent with our theoretical modeling and simulations. Moreover, the high-energy spin excitations around 14 meV agree with the one-pair spinon-antispinon excitations in Raman studies. The real part of the dynamical susceptibility derived from the Kramers-Kronig relationship also accords with the Knight shift measured by nuclear magnetic resonance, clearly demonstrating the negligible effects of magnetic impurities on static susceptibility. These results provide a rare example in studying quantum-spin-liquid materials where different experimental techniques can be directly compared and give further insights for the possible Dirac quantum spin liquid in this system.

A Dirac spinon is a kind of fractionalized excitations in quantum spin liquids (QSLs) that has been widely discussed in theories [1–5]. A Dirac spinon has spin 1/2 and is described by the Dirac equation, i.e., it is a fermion with linear dispersion, analogous to electrons in graphene but without the charge degree of freedom. One of the most promising models to study Dirac spinons is the antiferromagnetic (AFM) Heisenberg model on the kagome lattice [6–18]. Despite theoretical triumphs, the search for Dirac QSLs in the kagome materials has largely failed. One of the main reasons may be the existence of disorders and magnetic impurities in these materials [19–31], which may blur the sharp features of low-energy spin excitations in a Dirac QSL or even destroy it.

Recently, a new kagome system, $\text{YCu}_3(\text{OH})_6\text{Br}_2[\text{Br}_{1-x}(\text{OH})_x]$ ($\text{YCu}_3\text{-Br}$), has shown many interesting results that make it a promising QSL candidate [32–41]. Unlike many other kagome QSL candidates, this system shows no sign of magnetic impurities or weakly correlated spins. Heat capacity measurements clearly reveal behaviors expected for a Dirac QSL, including the quadratic temperature dependence of the specific heat at zero field and a linear term under fields [33]. More intriguingly, the spin excitations show cone continuum that may come from the convolution of two Dirac spinons [38]. These results show no sign of disorders and impurities, making $\text{YCu}_3\text{-Br}$ the best candidate

for the Dirac QSL so far. However, there are also several results that do not favor or even go against the existence of Dirac spinons. Thermal conductivity measurements do not observe a linear term that is supposed to exist in the presence of spinon Fermi surfaces coming from the Dirac spinons under fields [35]. Moreover, magnetic susceptibility shows almost no temperature dependence at low temperatures [33, 37, 42], whereas a linear temperature dependence is expected for a Dirac QSL. These results cast a shadow over the existence of Dirac spinons and has aroused alternate explanations [41]. It is worth noting that a one-ninth magnetization plateau and magnetic oscillations have been observed at about 20 T, and their origin is also debated [42–45].

In this work, we studied the spin excitations of $\text{YCu}_3(\text{OD})_6\text{Br}_2[\text{Br}_{0.33}(\text{OD})_{0.67}]$ using the inelastic neutron scattering (INS) technique. The temperature dependence and anisotropy of the low-energy spin excitations suggest finite quasiparticle lifetimes and the existence of Dzyaloshinskii-Moriya (DM) interaction. We argue that these factors explain the negative results from thermal conductivity and magnetic susceptibility measurements. Moreover, the dynamical susceptibility agrees excellently with Raman and NMR results, providing further evidence of the Dirac QSL in this system.

Single crystals of $\text{YCu}_3(\text{OD})_6\text{Br}_2[\text{Br}_{0.33}(\text{OD})_{0.66}]$ were grown using the hydrothermal method as reported pre-

viously [33]. Since the sample properties may vary among different batches [39], we have measured the low-temperature specific heats of the samples to make sure that the crystals used in the INS measurements exhibit the same properties [46]. About 800 single crystals with a mass of approximate 0.5 gram were co-aligned on a Cu plate using CYTOP, with a mosaic spread of about 3 degrees [46]. The momentum transfer Q in three-dimensional reciprocal space is defined as $Q = H\mathbf{a}^* + K\mathbf{b}^* + L\mathbf{c}^*$, where H , K and L are Miller indices and $\mathbf{a}^* = 2\pi(\mathbf{b} \times \mathbf{c})/V$, $\mathbf{b}^* = 2\pi(\mathbf{c} \times \mathbf{a})/V$ and $\mathbf{c}^* = 2\pi(\mathbf{a} \times \mathbf{b})/V$, with $a = b = 6.6779 \text{ \AA}$, $c = 5.9874 \text{ \AA}$, and $V = 231.23 \text{ \AA}^3$ of the kagome lattice. The crystal assembly was aligned in the $[H, 0, L]$ scattering plane. The unpolarized and polarized INS experiments were carried out on the cold-neutron disk chopper spectrometer AMATERAS at J-PARC [47] and the cold-neutron triple-axis spectrometer ThALES at ILL [48], respectively. All the spectral data of AMATERAS were processed by using the software suite Utseusemi [49]. In the polarized neutron experiment, an XYZ coil system is used for providing the needed guide fields at the sample, and the incoming neutron polarization directions are denoted as x , y , and z with x along the Q direction. While both y and z are perpendicular to Q , they are within and perpendicular to the scattering plane, respectively. After scattered by the sample, the outgoing neutron polarization can either parallel or antiparallel to the incoming neutron polarization, which corresponds to the nonspin flip (NSF) and spin flip (SF) processes, respectively. We also performed the theoretical modeling and employed the spin wave and the Landau-Lifshitz dynamics (LLD) simulation [50–52]. The computational details are given in the Supplemental Material (SM) [46].

As shown in our previous work [38], the spin excitations of $\text{YCu}_3\text{-Br}$ exhibit cone continua at six symmetrical positions within one Brillouin zone, among which the one at $(2/3, 0)$ has the strongest intensity. Figures 1(a) and 1(b) show the colormaps of the low-energy spin excitations as a function of E and Q along the $[H, 0]$ direction at 0.3 and 6 K, respectively. Similar to previous results, the cone continuum is clearly revealed at both $(2/3, 0)$ and $(4/3, 0)$ at 0.3 K. At 6 K, the cone continuum becomes column-like due to the significant broadening of low-energy spin excitations.

Figure 1(c) shows constant- E cuts at 0.1 meV at different temperatures, all of which can be well fitted by the Lorentzian function. The obtained temperature dependence of full-width-at-half-maximum (FWHM) is shown in Figs. 1(c) and 1(d), respectively. Interestingly, the FWHM at 0.1 meV changes linearly with T up to 6 K, with a slope of about $0.0211 \pm 0.003 \text{ \AA}^{-1}/\text{K}$, while those above 0.5 meV show little temperature dependence. This behavior may be resulted from the spinon-spinon interaction near Dirac points. It is well known that the inverse inelastic quasiparticle lifetime τ^{-1} near the Dirac nodes

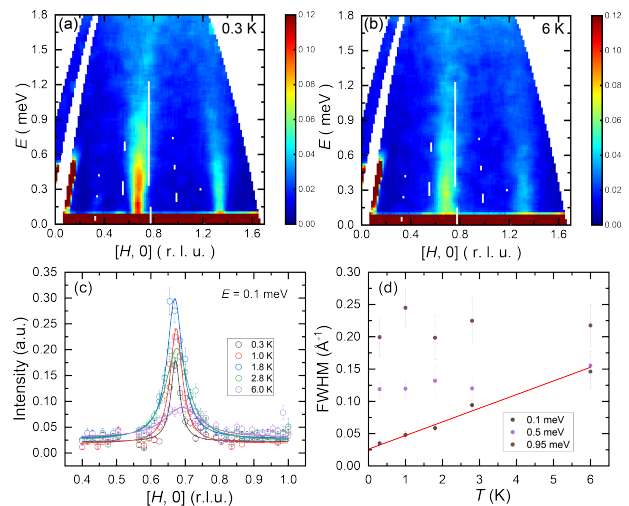


FIG. 1. (a) and (b) Intensity contour plots of the INS results as a function of E and Q along the $[H, 0]$ direction at 0.3 and 6 K, respectively, with $E_i = 2.57$ meV. (c) Constant- E cuts along the $[H, 0]$ direction at 0.1 meV at various temperatures. The solid lines are fitted results by the Lorentzian function. The integrated ranges of the energy and $[-0.5K, K]$ are ± 0.05 meV and ± 0.1 r.l.u., respectively. (d) Temperature dependence of the FWHM. The solid line is the linear-fit result at 0.1 meV. In all figures, r.l.u. is the reciprocal lattice unit.

in the intrinsic undoped graphene is linear with both temperature and energy due to electron-electron interaction [53]. We argue that the same mechanism may also work for Dirac spinons, so the energy width ΔE of the Dirac dispersion is linear with both temperature and energy, too, as $\Delta E \sim \tau^{-1}\hbar/2$. Because INS experiments detect two-spinon excitations, the momentum width ΔQ at low energies is also linear with temperature as $\Delta E \sim \hbar\nu_F\Delta Q$, where ν_F is the spinon velocity.

To further reveal the nature of the low-energy spin excitations, we also carried out polarized INS measurements in the $[H, 0, L]$ plane, as illustrated in Fig. 2(a). Since neutrons only detect magnetic scattering components perpendicular to Q , we can obtain magnetic responses along the y and z directions, denoted as M_y and M_z , respectively. Accordingly [54], we obtain

$$M_y = \frac{R+1}{R-1}(\sigma_x^{SF} - \sigma_y^{SF}), \quad (1)$$

$$M_z = \frac{R+1}{R-1}(\sigma_x^{SF} - \sigma_z^{SF}), \quad (2)$$

where σ_x^{SF} , σ_y^{SF} , and σ_z^{SF} are the SF scattering cross sections for the corresponding neutron polarization direction, and R is the flipping ratio between NSF and SF scattering. R is large (> 15) so the flipping-ratio correction term can be neglected. As shown in Fig. 2(b), for magnetic intensities of excitations within the ab plane (M_{ab}) and along the c axis (M_c), we obtain $M_z = M_{ab}$ and $M_y = M_{ab} \sin^2 \theta + M_c \cos^2 \theta$, where θ is the angle

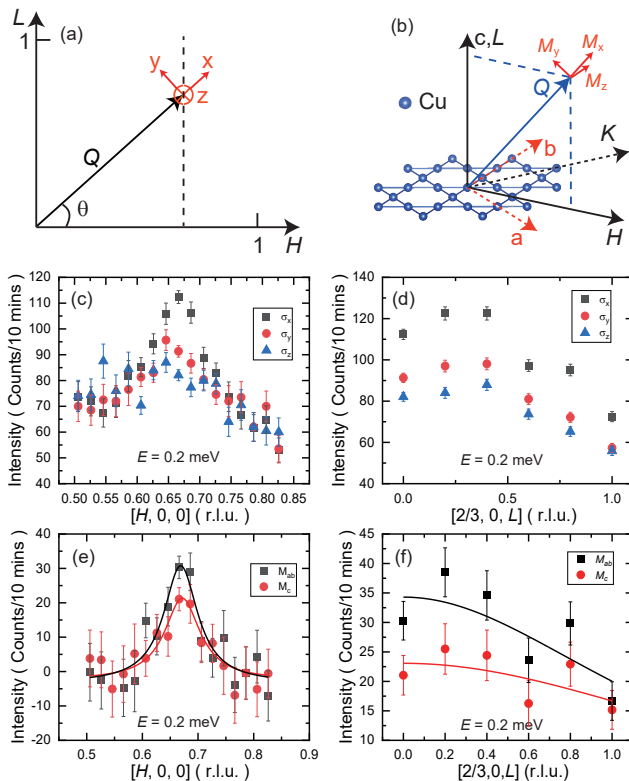


FIG. 2. (a) and (b) Illustration of the neutron polarized measurement in the $[H,0,L]$ plane and real space. The x , y , and z are the neutron polarization directions. The angle between Q and the $(H,0,0)$ direction is denoted as θ . (c), (d) Constant- E scans at 0.2 meV along the $[H,0,0]$ and $[2/3,0,L]$ directions, respectively. (e), (f) In-plane and out-of-plane magnetic responses (M_{ab} and M_c) at 0.2 meV along the $[H,0,0]$ and $[2/3,0,L]$ directions, respectively. The solid lines in (e) are fitted by a Lorentzian function. The solid lines in (f) are guides by the eye. All measurements in this figure were carried out at about 50 mK and with a fixed $k_f = 1.3 \text{ \AA}^{-1}$.

between Q and the $(H,0,0)$ direction. Here, we focus on the spin excitations at 0.2 meV and 50 mK around $(2/3,0,0)$. Figures 2(c) and 2(d) show scans along the $[H,0,0]$ and $[2/3,0,L]$ directions for all three SF channels, respectively. The corresponding M_{ab} and M_c can thus be obtained as shown in Figs. 2(e) and 2(f). In both cases, the ratio of M_{ab}/M_c is very close to 1.5. We note that this anisotropy can not be due to the anisotropic g -factor since g_{ab}/g_c is slightly smaller than 1 as shown by the magnetization measurements [33, 44].

In the following, we turn to the results of high-energy spin excitations. Figures 3(a) and 3(b) show high-energy spin excitations at 0.3 K along the $[H,0]$ and $[1-K/2,K]$ directions, respectively. In previous studies, the spin excitations were observed up to about 8 meV due to the incident energy limit [38], while here the excitations have been found up to approximately 18 meV with $E_i = 21.91$ meV. Whether there are spin excitations at even higher

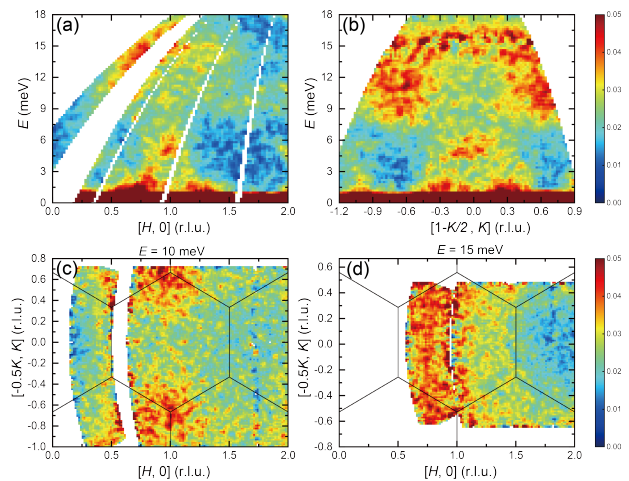


FIG. 3. (a) and (b) Intensity contour plots of the INS results as a function of E and Q along the $[H,0]$ and $[1-K/2,K]$ directions, respectively, with $E_i = 21.91$ meV and $T = 0.3$ K. The corresponding integrated range along the $[-K/2, K/2]$ and $[H,0]$ directions are from $K = -0.12$ to $K = 0.12$ and from $H = 0.9$ to $H = 1.1$, respectively. (c) Intensity contour plot of the INS results within the $[H,K]$ plane at 10 and 15 meV, respectively, at $T = 0.3$ K. The integrated energy range is 2 meV. The solid lines are the kagome Brillouin zone.

energies need to be further studied. Similar to previous results [38], the low-energy spin excitations at $(2/3,0)$ and the symmetrical positions gradually merge together at the zone center $(1,0)$ below about 8 meV. At higher energies, new excitations emerge from the zone corners, i.e., $(2/3,2/3)$ and $(4/3,-2/3)$, as further shown in Fig. 3(c). These locations correspond to the K points in the Brillouin zone [see the inset of Fig. 4(a)]. When the energy increases to about 15 meV, the spin excitations are observed throughout the Brillouin zone [Fig. 3(d)]. Note that the $|Q|$ dependence of the intensity at 15 meV can be fitted by a cosine function analogous to the structure factor of randomly arranged nearest-neighbour singlets together with the magnetic form factor of Cu^{2+} [46], which results in seemingly higher intensities at smaller Q 's.

Previous Raman scattering has revealed high-energy magnetic excitations that are suggested to come from one-pair (1P) and two-pair (2P) spinon-antispinon excitations [43]. Here, we plot the intensity of our high-energy spin excitations together with the 1P Raman susceptibility in the A_{1g} channel in Fig. 4(a). Note that we have combined the neutron data at different temperatures since the high-energy spin excitations are essentially temperature-independent for the temperature range measured here ($T \leq 6$ K). A broad peak is found in neutron scattering data at about 14 meV at the K point, similar to the peak in Raman 1P excitations, suggesting their common origin. Note that the Raman scattering technique detects spinon-antispinon pairs with a

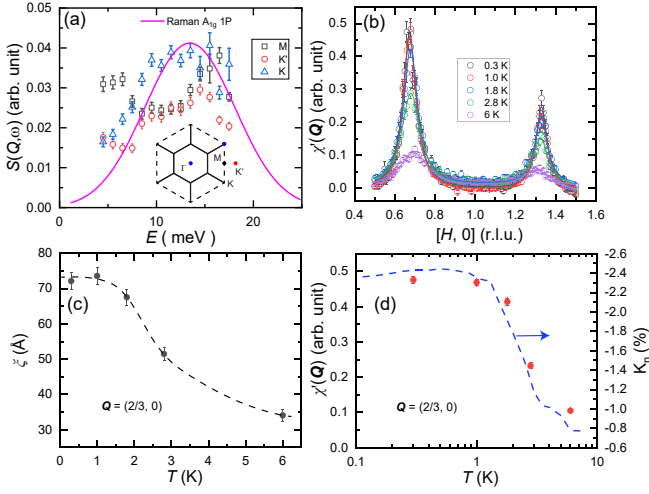


FIG. 4. (a) Energy dependence of $S(Q, \omega)$ above 4 meV. The solid line represents Raman magnetic susceptibility for 1P spinon-antispinon excitations in the A_{1g} channel [43]. The inset shows kagome (solid lines) and extended (dashed lines) Brillouin zones with high-symmetry points. (b) $\chi'(Q)$ along the $[H, 0]$ direction at several temperatures. The solid lines are fitted results by the Lorentzian function. (c) Temperature dependence of magnetic correlation length ξ at $Q = (2/3, 0)$. The dashed line is a guide to the eye. (d) Temperature dependence of $\chi'(Q)$ at $Q = (2/3, 0)$. The dashed blue line is the Knight shift from the NMR measurements [37].

total spin quantum number $\Delta S = 0$, while INS measures two spinon excitations with $\Delta S = \pm 1$ [55]. The probability of two excited spinons with the same and opposite spin quantum numbers could be same so that the results of Raman and neutron scattering are consistent. These excitations also exist at the M and K' points, but are significantly enhanced with decreasing energy compared with Raman susceptibility. Note that Raman spectroscopy only detects signal at Γ ($Q = 0$), so its results cannot be directly compared with the low-energy spin excitations measured by the INS technique at finite Q 's.

As shown previously, we can obtain the real part of the dynamical susceptibility $\chi'(Q)$ from the Kramers-Kronig relationship [38]. Figure 4(b) shows $\chi'(Q)$ along the $[H, 0]$ direction at various temperatures. The peaks at $(2/3, 0)$ and $(4/3, 0)$ become much broader and lower at 6 K compared to those at low temperatures. The magnetic correlation length ξ at $(2/3, 0)$ can be calculated as $\xi = 2\pi/w$, where w is the full width at half maximum (FWHM) of the $\chi'(Q)$ peak at $(2/3, 0)$ fitted by the Lorentzian function. Figure 4(c) shows the temperature dependence of ξ , which increases with decreasing T and saturates below about 1 K. This seems to accord with the loss of T^2 dependence in the specific heat above 1 K [33, 46]. Figure 4(d) shows the temperature dependence of the peak intensity $\chi'(Q)$ at $(2/3, 0)$, which also becomes saturated below about 1 K. Note that the Knight shift $^{81}K_n$ obtained from the nuclear magnetic resonance

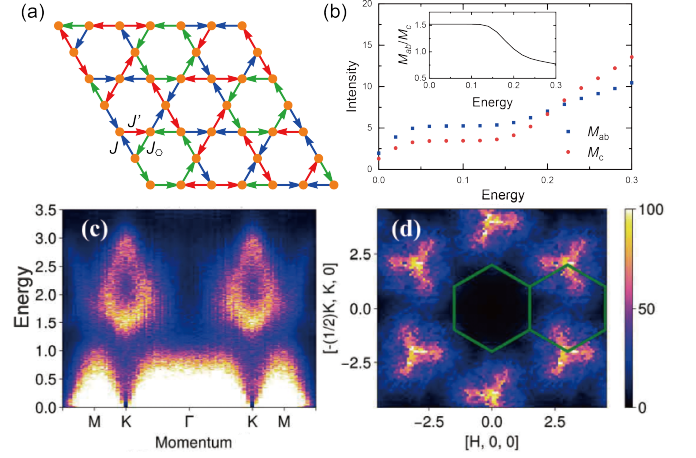


FIG. 5. (a) A sketch for the theoretical model – 3J model (referring to fact that we need 3 antiferromagnetic couplings), including definition of different bonds, J , J' , and J_\square . The arrows show the definition of the bond orientations $\langle i, j \rangle$ that determine the sign of DM interactions in the Hamiltonian. (b) Energy dependence of calculated M_{ab} and M_c with Q integrated around K' position. The inset shows the ratio M_{ab}/M_c . Here $\alpha = 0.4$ and $\Delta = 0.7$. D is assumed to have a randomness from 0.03 to 0.07. (c) Contour plots of the calculated spin excitations as a function of energy and momentum along the high symmetrical points as defined in Fig. 3(a). Here $\alpha = 0.6$ and $D = 0$. (d) In-plane contour plots of the calculated spin excitations at $E = 1.5$. The solid lines represent the kagome Brillouin zone.

(NMR) spectroscopy shows similar behavior [37].

The anisotropic low-energy spin excitations and the high-energy spin excitations above 8 meV provide new information to understand the spin system in $YCu_3\text{-Br}$. The anisotropy suggests the existence of non-Heisenberg interactions in this system. A highly possible candidate is the DM interaction, which has been shown to exist in other similar kagome materials, such as herbertsmithite and $YCu_3(\text{OH})_6\text{Cl}_3$ [56–58]. To illustrate the effect of DM interaction on the spin excitations, we constructed a Hamiltonian as $H = \sum_{\langle i, j \rangle} J_{i, j} \mathbf{S}_i \cdot \mathbf{S}_j + \sum_{\langle i, j \rangle} \mathbf{D}_{i, j} \cdot (\mathbf{S}_i \times \mathbf{S}_j)$

where $J_{i, j}$ denotes nearest exchange energies given by J_\square , J , or J' as illustrated in Fig. 5(a), and $\mathbf{D}_{i, j}$ is the DM interaction. When $\mathbf{D}_{i, j} = 0$, the model can lead to a $Q = (1/3, 1/3)$ AFM order [59, 60]. While this model breaks the translational symmetry of the kagome lattice, it is shown to capture the Q positions of the low-energy spin excitations in $YCu_3\text{-Br}$ [38, 39]. For simplicity, we define $J = J_\square = J'/\alpha$, and the corresponding $\mathbf{D}_{i, j} = (\Delta D, \Delta D, D)$, with α and Δ parameters. We performed the spin wave and the Landau-Lifshitz dynamics (LLD) computation of the model (with the technical details given in SM [46]). Our results in Fig. 5(b) exhibit the consistent spectral weights in the low-energy spin spec-

trum, in that, the presence of the DM interaction in the model gives rise to the observed 1.5 ratio of M_{ab} over M_c as in Figs. 2(e) and 2(f), when the in-plane DM interaction is about 70% of that along c axis. The computed high-energy spectrum also capture the main feature of the experiment observation once the system enters the classical spin liquid regime [46]. The spectrum along the path of M - K - Γ are similar with those in Figs. 3(a) and 3(b). The constant high-energy cut in Fig. 5(d), highly resemble spectral weight distribution in Fig. 3(c) at 10 meV. We note these results suggest the effectiveness of the above model and simulation in capturing important experimental features, and a full quantum many-body treatment of our model for the Dirac QSL and its dynamical properties to understand the INS spectra, are now opened as promising directions.

It has been shown that the magnetic susceptibility and Knight shift do not decrease linearly with decreasing temperature when T approaches zero or increase linearly with increasing field at very low temperatures, which is against the picture for a Dirac QSL since they are supposed to be proportional to the density of states [33, 37, 41]. However, this assumption is true only when the spin rotation symmetry is preserved. We have shown the presence of DM interactions in our sample both experimentally and theoretically. Therefore, the magnetic susceptibility or Knight shift can no longer be considered effective tools to probe the ground states, as it has long been known that when the spin rotation symmetry is absent, the magnetic susceptibility tends to a constant at zero temperature, irrespective of the nature of low-energy excitations [1]. It is worth noting that the existence of DM interaction might be crucial for generating gauge field in this system [61].

Our results provide a rare example to directly compare INS data with Raman and NMR results in QSL candidates, as shown in Figs. 4(a) and 4(d), respectively. The consistency between the Knight shift and $\chi'[(Q = (2/3, 0))]$ confirms the dominant contribution of excitations at $(2/3, 0)$ at very low energies. It also clearly rules out magnetic impurities or strong disorders as the origin of low-temperature Knight shift or magnetic susceptibility. The consistency between Raman and INS spectra further supports the origin of the spin excitations above 8 meV as pairs of spinons. Compared to Raman scattering, our INS data revealed Q dependence of the high-energy spin excitations, which seems to emerge from the K positions in the extended Brillouin zone. The low-energy spin excitations cannot be described by the conventional kagome AFM model and their locations are consistent with the so-called $Q=(1/3, 1/3)$ magnetic order [59, 60]. The high-energy spin excitations are consistent with our theoretical calculations based on both the 3J and the traditional kagome AFM models [10, 59, 62, 63], where the intensity at K is higher than that at M when the energy large. These calculations are calling for more

theoretical and numerical studies on the model.

In conclusion, our results provide further evidence for the Dirac QSL in $YCu_3\text{-Br}$. The linear temperature dependence of the low-energy spin excitations suggests the existence of spinon-spinon interactions, analogous to those of Dirac electrons in graphene. Polarized INS reveals anisotropic low-energy spin excitations due to the existence of DM interactions, consistent with our theoretical calculations. High-energy excitations provide evidence for the existence of spinon pairs that are consistent with kagome AFM model. These results provide a harmonious picture across different experimental techniques and call for further theoretical studies.

We thank Y. Zhou, K. Jiang, Cristian Batista and Patrick Lee for helpful discussions. This work is supported by the National Key Research and Development Program of China (Grants No. 2022YFA1403400, No. 2021YFA1400400, 2023YFA1406100), the Chinese Academy of Sciences (Grants No. XDB33000000, No. GJTD-2020-01) and Research Grants Council of Hong Kong (Project Nos. 17309822, HKU C7037- 22GF, 17302223, 17301924). Measurements on AMATERAS were performed based on the approved proposal (Grant No. 2023B0063). We thank HPC2021 system under the Information Technology Services and the Blackbody HPC system at the Department of Physics, University of Hong Kong, as well as the Beijing PARATERA Tech CO.,Ltd. (URL:https://cloud.paratera.com) for providing HPC resources.

L.H., Z. Z., and C.Z. contributed equally to this work.

* kenji.nakajima@j-parc.jp

† y.su@fz-juelich.de

‡ slli@iphy.ac.cn

- [1] L. Savary and L. Balents, Quantum spin liquids: A review, *Rep. Prog. Phys.* **80**, 016502 (2017).
- [2] Y. Zhou, K. Kanoda, and T.-K. Ng, Quantum spin liquid states, *Rev. Mod. Phys.* **89**, 025003 (2017).
- [3] C. Broholm, R. J. Cava, S. A. Kivelson, D. G. Nocera, M. R. Norman, and T. Senthil, Quantum spin liquids, *Science* **367**, 263 (2020).
- [4] N. Ma, G.-Y. Sun, Y.-Z. You, C. Xu, A. Vishwanath, A. W. Sandvik, and Z. Y. Meng, Dynamical signature of fractionalization at a deconfined quantum critical point, *Phys. Rev. B* **98**, 174421 (2018).
- [5] X. Y. Xu, Y. Qi, L. Zhang, F. F. Assaad, C. Xu, and Z. Y. Meng, Monte carlo study of lattice compact quantum electrodynamics with fermionic matter: The parent state of quantum phases, *Phys. Rev. X* **9**, 021022 (2019).
- [6] M. B. Hastings, Dirac structure, RVB, and Goldstone modes in the kagomé antiferromagnet, *Phys. Rev. B* **63**, 014413 (2000).
- [7] M. Hermele, Y. Ran, P. A. Lee, and X.-G. Wen, Properties of an algebraic spin liquid on the kagome lattice, *Phys. Rev. B* **77**, 224413 (2008).
- [8] Y.-C. He, M. P. Zaletel, M. Oshikawa, and F. Pollmann,

- Signatures of dirac cones in a dmrg study of the kagome heisenberg model, *Phys. Rev. X* **7**, 031020 (2017).
- [9] W. Zhu, X. Chen, Y.-C. He, and W. Witczak-Krempa, Entanglement signatures of emergent Dirac fermions: Kagome spin liquid and quantum criticality, *Sci. Adv.* **4**, eaat5535 (2018).
- [10] W. Zhu, S. shu Gong, and D. N. Sheng, Identifying spinon excitations from dynamic structurefactor of spin-1/2 Heisenberg antiferromagnet on the kagome lattice, *Proc. Natl. Acad. Sci. U.S.A* **116**, 5437 (2019).
- [11] X.-Y. Song, C. Wang, A. Vishwanath, and Y.-C. He, Unifying description of competing orders in two-dimensional quantum magnets, *Nat. Commun.* **10**, 4254 (2019).
- [12] M. Hering, J. Sonnenschein, Y. Iqbal, and J. Reuther, Characterization of quantum spin liquids and their spinon band structures via functional renormalization, *Phys. Rev. B* **99**, 100405 (2019).
- [13] E. Dupuis, M. B. Paranjape, and W. Witczak-Krempa, Transition from a dirac spin liquid to an antiferromagnet: Monopoles in a qed₃-gross-neveu theory, *Phys. Rev. B* **100**, 094443 (2019).
- [14] X.-Y. Song, Y.-C. He, A. Vishwanath, and C. Wang, From spinon band topology to the symmetry quantum numbers of monopoles in Dirac spin liquids, *Phys. Rev. X* **10**, 011033 (2020).
- [15] Y. Iqbal, F. Ferrari, A. Chauhan, A. Parola, D. Poilblanc, and F. Becca, Gutzwiller projected states for the $J_1 - J_2$ heisenberg model on the kagome lattice: Achievements and pitfalls, *Phys. Rev. B* **104**, 144406 (2021).
- [16] D. Kiese, F. Ferrari, N. Astrakhantsev, N. Niggemann, P. Ghosh, T. Müller, R. Thomale, T. Neupert, J. Reuther, M. J. P. Gingras, S. Trebst, and Y. Iqbal, Pinch-points to half-moons and up in the stars: The kagome skymap, *Phys. Rev. Res.* **5**, L012025 (2023).
- [17] F. Ferrari, F. Becca, and R. Valentí, Spin-phonon interactions on the kagome lattice: Dirac spin liquid versus valence-bond solids, *Phys. Rev. B* **109**, 165133 (2024).
- [18] U. F. P. Seifert, J. Willsher, M. Drescher, F. Pollmann, and J. Knolle, Spin-peierls instability of the U(1) Dirac spin liquid, *Nat. Commun.* **15**, 7110 (2024).
- [19] M. A. de Vries, K. V. Kamenev, W. A. Kockelmann, J. Sanchez-Benitez, and A. Harrison, Magnetic ground state of an experimental $S = 1/2$ kagome antiferromagnet, *Phys. Rev. Lett.* **100**, 157205 (2008).
- [20] D. E. Freedman, T. H. Han, A. Prodi, P. Müller, Q.-Z. Huang, Y.-S. Chen, S. M. Webb, Y. S. Lee, T. M. McQueen, and D. G. Nocera, Site specific x-ray anomalous dispersion of the geometrically frustrated kagomé magnet, herbertsmithite, $\text{ZnCu}_3(\text{OH})_6\text{Cl}_2$, *J. Am. Chem. Soc.* **132**, 16185 (2010).
- [21] Y. Y. Huang, Y. Xu, L. Wang, C. C. Zhao, C. P. Tu, J. M. Ni, L. S. Wang, B. L. Pan, Y. Fu, Z. Hao, C. Liu, J.-W. Mei, and S. Y. Li, Heat transport in herbertsmithite: Can a quantum spin liquid survive disorder?, *Phys. Rev. Lett.* **127**, 267202 (2021).
- [22] T. H. Han, J. S. Helton, S. Chu, D. G. Nocera, J. A. Rodriguez-Rivera, C. Broholm, and Y. S. Lee, Fractionalized excitations in the spin-liquid state of a kagome-lattice antiferromagnet, *Nature* **492**, 406 (2012).
- [23] M. Fu, T. Imai, T.-H. Han, and Y. S. Lee, Evidence for a gapped spin-liquid ground state in a kagome heisenberg antiferromagnet, *Science* **350**, 655 (2015).
- [24] T.-H. Han, M. R. Norman, J.-J. Wen, J. A. Rodriguez-Rivera, J. S. Helton, C. Broholm, and Y. S. Lee, Correlated impurities and intrinsic spin-liquid physics in the kagome material herbertsmithite, *Phys. Rev. B* **94**, 060409 (2016).
- [25] P. Khuntia, M. Velazquez, Q. Barthélemy, F. Bert, E. Kermarrec, A. Legros, B. Bernu, A. Z. L. Messio, and P. Mendels, Gapless ground state in the archetypal quantum kagome antiferromagnet $\text{ZnCu}_3(\text{OH})_6\text{Cl}_2$, *Nat. Phys.* **16**, 469 (2020).
- [26] Z. Feng, Z. Li, X. Meng, W. Yi, Y. Wei, J. Zhang, Y.-C. Wang, W. Jiang, Z. Liu, S. Li, F. Liu, J. Luo, S. Li, G. qing Zheng, Z. Y. Meng, J.-W. Mei, and Y. Shi, Gapped spin-1/2 spinon excitations in a new kagome quantum spin liquid compound $\text{Cu}_3\text{Zn}(\text{OH})_6\text{FBr}$, *Chin. Phys. Lett.* **34**, 077502 (2017).
- [27] Y. Wei, Z. Feng, W. Lohstroh, D. H. Yu, D. Le, C. dela Cruz, W. Yi, Z. F. Ding, J. Zhang, C. Tan, L. Shu, Y.-C. Wang, H.-Q. Wu, J. Luo, J.-W. Mei, F. Yang, X.-L. Sheng, W. Li, Y. Qi, Z. Y. Meng, Y. Shi, and S. Li, Evidence for the topological order in a kagome antiferromagnet, arXiv e-prints, arXiv:1710.02991 (2017), arXiv:1710.02991 [cond-mat.str-el].
- [28] Z. Feng, W. Yi, K. Zhu, Y. Wei, S. Miao, J. Ma, J. Luo, S. Li, Z. Y. Meng, and Y. Shi, From claringbullite to a new spin liquid candidate $\text{Cu}_3\text{Zn}(\text{OH})_6\text{FCl}$, *Chin. Phys. Lett.* **36**, 017502 (2018).
- [29] Y. Fu, M.-L. Lin, L. Wang, Q. Liu, L. Huang, W. Jiang, Z. Hao, C. Liu, H. Zhang, X. Shi, J. Zhang, J. Dai, D. Yu, F. Ye, P. A. Lee, P.-H. Tan, and J.-W. Mei, Dynamic fingerprint of fractionalized excitations in single-crystalline $\text{Cu}_3\text{Zn}(\text{OH})_6\text{FBr}$, *Nature Communications* **12**, 3048 (2021).
- [30] Y. Wei, X. Ma, Z. Feng, Y. Zhang, L. Zhang, H. Yang, Y. Qi, Z. Y. Meng, Y.-C. Wang, Y. Shi, and S. Li, Non-local effects of low-energy excitations in quantum-spin-liquid candidate $\text{Cu}_3\text{Zn}(\text{OH})_6\text{FBr}$, *Chin. Phys. Lett.* **38**, 097501 (2021).
- [31] M. R. Norman, Colloquium: Herbertsmithite and the search for the quantum spin liquid, *Rev. Mod. Phys.* **88**, 041002 (2016).
- [32] X.-H. Chen, Y.-X. Huang, Y. Pan, and J.-X. Mia, Quantum spin liquid candidate $\text{YCu}_3(\text{OH})_6\text{Br}_2[\text{Br}_x(\text{OH})_{1-x}]$ ($x \approx 0.51$): With an almost perfect kagomé layer, *J. Magn. Magn. Mater.* **512**, 167066 (2020).
- [33] Z. Zeng, X. Ma, S. Wu, H.-F. Li, Z. Tao, X. Lu, X.-h. Chen, J.-X. Mi, S.-J. Song, G.-H. Cao, G. Che, K. Li, G. Li, H. Luo, Z. Y. Meng, and S. Li, Possible Dirac quantum spin liquid in the kagome quantum antiferromagnet $\text{YCu}_3(\text{OH})_6\text{Br}_2[\text{Br}_x(\text{OH})_{1-x}]$, *Phys. Rev. B* **105**, L121109 (2022).
- [34] J. Liu, L. Yuan, X. Li, B. Li, K. Zhao, H. Liao, and Y. Li, Gapless spin liquid behavior in a kagome heisenberg antiferromagnet with randomly distributed hexagons of alternate bonds, *Phys. Rev. B* **105**, 024418 (2022).
- [35] X. Hong, M. Behnami, L. Yuan, B. Li, W. Brenig, B. Büchner, Y. Li, and C. Hess, Heat transport of the kagome Heisenberg quantum spin liquid candidate $\text{YCu}_3(\text{OH})_{6.5}\text{Br}_{2.5}$: Localized magnetic excitations and a putative spin gap, *Phys. Rev. B* **106**, L220406 (2022).
- [36] F. Lu, L. Yuan, J. Zhang, B. Li, Y. Luo, and Y. Li, The observation of quantum fluctuations in a kagome Heisenberg antiferromagnet, *Commun. Phys.* **5**, 272 (2022).
- [37] S. Li, Y. Cui, Z. Zeng, Y. Wang, Z. Hu, J. Liu, C. Li, X. Xu, Y. Chen, Z. Liu, S. Li, and W. Yu, Nmr evidence of spinon localization in the kagome antiferro-

- magnet $\text{YCu}_3(\text{OH})_6\text{Br}_2[\text{Br}_{1-x}(\text{OH})_x]$, *Phys. Rev. B* **109**, 104403 (2024).
- [38] Z. Zeng, C. Zhou, H. Zhou, L. Han, R. Chi, K. Li, M. Kofu, K. Nakajima, Y. Wei, W. Zhang, D. G. Mazzone, Z. Y. Meng, and S. Li, Spectral evidence for dirac spinons in a kagome lattice antiferromagnet, *Nat. Phys.* **20**, 1097 (2024).
- [39] A. Xu, Q. Shen, B. Liu, Z. Zeng, L. Han, L. Yan, J. Luo, J. Yang, R. Zhou, and S. Li, Magnetic ground states in the kagome system $\text{ycu}_3(\text{OH})_6[(\text{Cl}_x\text{Br}_{1-x})_{3-y}(\text{OH})_y]$, *Phys. Rev. B* **110**, 085146 (2024).
- [40] B. S. Shivaram, J. C. Prestigiacomo, A. Xu, Z. Zeng, T. D. Ford, I. Kimchi, S. Li, and P. A. Lee, Nonanalytic magnetic response and intrinsic ferromagnetic clusters in a kagome spin-liquid candidate, *Phys. Rev. B* **110**, L121105 (2024).
- [41] S. Suetsugu, T. Asaba, S. Ikemori, Y. Sekino, Y. Kasahara, K. Totsuka, B. Li, Y. Zhao, Y. Li, Y. Kohama, and Y. Matsuda, Gapless spin excitations in a quantum spin liquid state of $s=1/2$ perfect kagome antiferromagnet (2024), arXiv:2407.16208.
- [42] S. Suetsugu, T. Asaba, Y. Kasahara, Y. Kohsaka, K. Totsuka, B. Li, Y. Zhao, Y. Li, M. Tokunaga, and Y. Matsuda, Emergent spin-gapped magnetization plateaus in a spin-1/2 perfect kagome antiferromagnet, *Phys. Rev. Lett.* **132**, 226701 (2024).
- [43] S. Jeon, D. Wulferding, Y. Choi, S. Lee, K. Nam, K. H. Kim, M. Lee, T.-H. Jang, J.-H. Park, S. Lee, S. Choi, C. Lee, H. Nojiri, and K.-Y. Choi, One-ninth magnetization plateau stabilized by spin entanglement in a kagome antiferromagnet, *Nat. Phys.* **20**, 435 (2024).
- [44] G. Zheng, Y. Zhu, K.-W. Chen, B. Kang, D. Zhang, K. Jenkins, A. Chan, Z. Zeng, A. Xu, O. A. Valenzuela, J. Blawat, J. Singleton, P. A. Lee, S. Li, and L. Li, Unconventional magnetic oscillations in kagome Mott insulators (2023), arXiv:2310.07989.
- [45] G. Zheng, D. Zhang, Y. Zhu, K.-W. Chen, A. Chan, K. Jenkins, B. Kang, Z. Zeng, A. Xu, D. Ratkovski, J. Blawat, A. Bangura, J. Singleton, P. A. Lee, S. Li, and L. Li, Thermodynamic evidence of fermionic behavior in the vicinity of one-ninth plateau in a kagome antiferromagnet (2024), arXiv:2409.05600.
- [46] In this Supplemental Material, we provide the details of experimental results and the modeling of the material and its solution based on the Langevin dynamic numerical simulations.
- [47] K. Nakajima, S. Ohira-Kawamura, T. Kikuchi, M. Nakamura, R. Kajimoto, Y. Inamura, N. Takahashi, K. Aizawa, K. Suzuya, K. Shibata, T. Nakatani, K. Soyama, R. Maruyama, H. Tanaka, W. Kambara, T. Iwahashi, Y. Itoh, T. Osakabe, S. Wakimoto, K. Kakurai, F. Maekawa, M. Harada, K. Oikawa, R. E. Lechner, F. Mezei, and M. Arai, AMATERAS: A cold-neutron disk chopper spectrometer, *J. Phys. Soc. Jpn.* **80**, SB028 (2011).
- [48] M. Boehm, A. Hiess, J. Kulda, S. Roux, and J. Saroun, ThALES—three axis low energy spectroscopy at the Institut Laue-Langevin, *Meas. Sci. Technol.* **19**, 034024 (2008).
- [49] Y. Inamura, T. Nakatani, J. Suzuki, and T. Otomo, Development status of software 'Utsusemi' for chopper spectrometers at MLF, J-PARC, *J. Phys. Soc. Jpn.* **82**, SA031 (2013).
- [50] D. Dahlbom, C. Miles, H. Zhang, C. D. Batista, and K. Barros, Langevin dynamics of generalized spins as $\text{su}(n)$ coherent states, *Phys. Rev. B* **106**, 235154 (2022).
- [51] D. Dahlbom, H. Zhang, C. Miles, X. Bai, C. D. Batista, and K. Barros, Geometric integration of classical spin dynamics via a mean-field schrödinger equation, *Phys. Rev. B* **106**, 054423 (2022).
- [52] H. Zhang and C. D. Batista, Classical spin dynamics based on $\text{SU}(n)$ coherent states, *Phys. Rev. B* **104**, 104409 (2021).
- [53] Q. Li and S. Das Sarma, Finite temperature inelastic mean free path and quasiparticle lifetime in graphene, *Phys. Rev. B* **87**, 085406 (2013).
- [54] L. P. Regnault, Inelastic neutron polarization analysis, in *Neutron Scattering from Magnetic Materials*, edited by T. Chatterji (Elsevier B.V., 2006) Chap. 8, pp. 363–395.
- [55] Strictly speaking, it is not clear whether neutron scattering can detect two spinon excitations with a total $S = 0$ or not, but the argument in the text holds in both cases.
- [56] O. Cépas, C. M. Fong, P. W. Leung, and C. Lhuillier, Quantum phase transition induced by Dzyaloshinskii-Moriya interactions in the kagome antiferromagnet, *Phys. Rev. B* **78**, 140405 (2008).
- [57] A. Zorko, S. Nellutla, J. van Tol, L. C. Brunel, F. Bert, F. Duc, J.-C. Trombe, M. A. de Vries, A. Harrison, and P. Mendels, Dzyaloshinsky-moriya anisotropy in the spin-1/2 kagome compound $\text{zncu}_3(\text{OH})_6\text{cl}_2$, *Phys. Rev. Lett.* **101**, 026405 (2008).
- [58] T. Arh, M. Gomilšek, P. Prelovšek, M. Pregelj, M. Klanjšek, A. Ozarowski, S. J. Clark, T. Lancaster, W. Sun, J.-X. Mi, and A. Zorko, Origin of magnetic ordering in a structurally perfect quantum kagome antiferromagnet, *Phys. Rev. Lett.* **125**, 027203 (2020).
- [59] M. Hering, F. Ferrari, A. Razpopov, I. I. Mazin, R. Valentí, H. O. Jeschke, and J. Reuther, Phase diagram of a distorted kagome antiferromagnet and application to Y-kapellasite, *npj Comput. Mater.* **8**, 10 (2022).
- [60] D. Chatterjee, P. Puphal, Q. Barthélemy, J. Willwarter, S. Süllow, C. Baines, S. Petit, E. Ressouche, J. Olivier, K. M. Zoch, C. Krellner, M. Parzer, A. Riss, F. Garmroudi, A. Pustogow, P. Mendels, E. Kermarrec, and F. Bert, From spin liquid to magnetic ordering in the anisotropic kagome Y-kapellasite $\text{Y}_3\text{Cu}_9(\text{OH})_{19}\text{Cl}_8$: A single-crystal study, *Phys. Rev. B* **107**, 125156 (2023).
- [61] B. Kang and P. A. Lee, Generation of gauge magnetic fields in a kagome spin liquid candidate using the Dzyaloshinskii-Moriya interaction (2024), arXiv:2401.01946.
- [62] M. Punk, D. Chowdhury, and S. Sachdev, Topological excitations and the dynamic structure factor of spin liquids on the kagome lattice, *Nat. Phys.* **10**, 289 (2014).
- [63] F. Ferrari, S. Niu, J. Hasik, Y. Iqbal, D. Poilblanc, and F. Becca, Static and dynamical signatures of Dzyaloshinskii-Moriya interactions in the heisenberg model on the kagome lattice, *SciPost Phys.* **14**, 139 (2023).